Superbandwidth laser pulses in a dispersive medium: Oscillating beyond the Fourier spectrum with unexpected propagation features

Enrique G. Neyra,[1,*] Laureano A. Bulus Rossini,[1] Fabián Videla,[2,3] Lorena Rebón,[4,5,†] and Pablo A. Costanzo Caso[1]

[1]*Instituto Balseiro (Universidad Nacional de Cuyo and Comisión Nacional de Energía Atómica) and CONICET CCT Patagonia Norte. Av. Bustillo 9500, Bariloche 8400 (RN), Argentina*

[2]*Centro de Investigaciones Ópticas (CICBA-CONICET-UNLP), Cno. Parque Centenario y 506, P.O. Box 3, 1897 Gonnet, Argentina*

[3]*Departamento de Ciencias Básicas, Facultad de Ingeniería UNLP, 1 y 47, 1900 La Plata, Argentina*

[4]*Departamento de Física, FCE, Universidad Nacional de La Plata, C.C. 67, 1900 La Plata, Argentina*

[5]*Instituto de Física de La Plata, UNLP-CONICET, Diagonal 113, entre 63 y 64, 1900 La Plata, Argentina*

(Received 2 November 2023; accepted 12 April 2024; published 6 May 2024)

The concept of superbandwidth refers to the fact that a band-limited signal can exhibit, locally, an increase of its bandwidth, i.e., an effective bandwidth greater than that predicted by its Fourier transform. In this work, we study the propagation of superbandwidth laser pulses in a dispersive medium, characterized by the group velocity dispersion. In particular, two important results arise from the analysis of the instantaneous frequency of the pulse obtained through the Wigner function distribution. First, local oscillations of the electric field which are beyond the Fourier spectrum of the incoming pulse can be observed. Second, for a range of values of the pulse synthesis parameters, surprisingly, the dynamics of the instantaneous frequency within certain temporal regions, corresponds to that of a pulse propagating in a medium with a group velocity dispersion of opposite sign. This phenomenon is intrinsic to the special characteristics of the pulse and not to the dispersive properties of the medium.

DOI: 10.1103/PhysRevA.109.053507

I. INTRODUCTION

Wave phenomena are perhaps the most frequent physical phenomena in nature. They are present in all branches of physics, from quantum mechanics to general relativity, and together with the superposition principle, play a key role in the description of the universe. Therefore, the wave phenomenon known as superoscillations has gained attention in the area of classical optics and beyond [1].

Superoscillations occur when a band-limited function locally oscillates faster than the highest frequency in its Fourier spectrum, which can be accomplished by manipulating the spectral phase of such a function to cause destructive interference between Fourier components. This phenomenon was initially studied in a purely mathematical framework [2,3], to later find real applications to subdiffractive beams [4–7], signal processing [8,9], ultrashort pulses [10,11], acoustic waves [12,13], among others [14–18].

In this context, we present two equivalent techniques to obtain subdiffractive Gaussian beams through the destructive interference of two pulses with different spatial widths [19]. After considering the mathematical equivalence between Gaussian beams and ultrashort pulses, the same idea was implemented to obtain sub-Fourier ultrashort pulses [20]. In the temporal domain, these techniques generate an ultrashort pulse with a central temporal lobe whose full width at half maximum (FWHM) is below the Fourier limit. Subsequently, in Ref. [21], we introduced the wave phenomenon of *superbandwidth* (SB), in which these sub-Fourier laser pulses interact locally with matter as if they had a spectral bandwidth greater than that predicted by the Fourier transform. In other words, the SB pulse interacts as if it had frequencies higher and lower than those present in its Fourier spectrum [22].

As is known, when a laser pulse $E(t)$ propagates in a dispersive medium (DM), it spreads temporally since each frequency within its spectrum travels at a different speed. At first order, this phenomenon is described by the group velocity dispersion (GVD) [23], which we will characterize by the parameter β_2. In the case where the medium has a positive (negative) dispersion, i.e., $\beta_2 > 0$ ($\beta_2 < 0$), lower frequencies travel faster (slower) than the higher ones. Moreover, as a DM allows to decompose the spectral content of a Fourier-limited laser pulse along the time axis as it travels through such a medium, the GVD produces the temporal Fourier transform, when the pulse propagates a long distance [24,25]. Thus, the possibility of controlling and manipulating both the sign and value of GVD through different devices such as prisms [26], diffraction gratings [27], or chirped mirrors [28] is essential in ultrafast optics [29,30] and strong-field laser physics [31].

In this work, we theoretically study the propagation of a SB laser pulse in a DM. The laser pulse is represented by a linear operator which introduces a quadratic phase $H_D(\omega) = e^{-i\Omega(\omega-\omega_0)^2}$, where $\Omega = \frac{1}{2}\beta_2 \times z$ and z is the propagation distance. Although the medium is linear and the synthesis of the

*enriqueneyra@cnea.gob.ar
†rebon@fisica.unlp.edu.ar

SB pulse can be obtained by a simple experimental technique, the instantaneous frequency of such a pulse, $\omega(t) = \frac{d\phi(t)}{dt}$, as it travels through the medium exhibits a very complex and physically rich behavior. First, we will report the existence of local oscillations of the electric field, represented by $\omega(t)$, which appear when the SB pulse propagates through the medium. Within some temporal window, these oscillations are beyond the Fourier spectrum of the original pulse. Second, we will show that, in a range of values of the parameters that control the synthesis of the SB pulse, surprisingly, $\omega(t)$ behaves as if the pulse were traveling in a medium with a GVD of opposite sign. Both effects disappear when the propagation distance is large enough, and the frequency $\omega(t)$, as given by the Fourier spectrum, is recovered.

II. RESULTS

We will start by defining the SB pulses analyzed in this work, which are similar to those studied in Ref. [22]. These pulses arises from the destructive interference between two Gaussian pulses with different amplitudes and temporal widths, which can be easily synthesized using an interferometric system. In the spectral domain, the SB pulses are described by the expression

$$\tilde{E}_{\rm SB}(\omega) = e^{-(\frac{\omega-\omega_0}{\Delta\omega})^2} - \alpha e^{-(\frac{\omega-\omega_0}{\beta\Delta\omega})^2}, \tag{1}$$

where the first term $\tilde{E}_G(\omega) = e^{-(\frac{\omega-\omega_0}{\Delta\omega})^2}$ corresponds to the electric field of the initial Gaussian pulse with normalized unit amplitude, which travels, unchanged, through the interferometer. In this context, ω_0 and $\Delta\omega$ denote its carrier frequency and bandwidth, respectively. The second term in Eq. (1), stands for the pulse that was modified before recombination. A theoretical analysis on the reduction of the temporal FWHM of the central lobe of the SB pulse, as a function of α and β, can be found in Ref. [19]. Consequently, the synthesized SB pulse when propagating through a DM, can be expressed as

$$\begin{aligned} E^D_{\rm SB}(t) \equiv \left|E^D_{\rm SB}(t)\right| e^{i\phi(t)} &= \mathcal{F}\left[\tilde{E}^D_{\rm SB}(\omega)\right] \\ &= \mathcal{F}\left[\tilde{E}_{\rm SB}(\omega) e^{-i\Omega(\omega-\omega_0)^2}\right]. \end{aligned} \tag{2}$$

In what follows, we will resort to the Wigner function formalism, which allows for a time-frequency analysis to study the dynamics of pulse propagation through DMs [32,33], and provides a more complete interpretation of the physics behind the phenomenon (see Appendix A for the analysis made through the Wigner function distribution that reveals the different propagation features.) For instance, starting from the representation of the field in the frequency domain, the Wigner function distribution in the time-frequency phase space is defined as

$$W(t,\omega) = \frac{1}{2\pi}\int_{-\infty}^{\infty} \tilde{E}(\omega + s/2)\tilde{E}^*(\omega - s/2)e^{its}ds, \tag{3}$$

from where, by replacing the mathematical expression of the field under consideration, the instantaneous frequency can be obtained as the average

$$\omega(t) = \frac{\int_{-\infty}^{\infty} \omega W(t,\omega)d\omega}{\int_{-\infty}^{\infty} W(t,\omega)d\omega}. \tag{4}$$

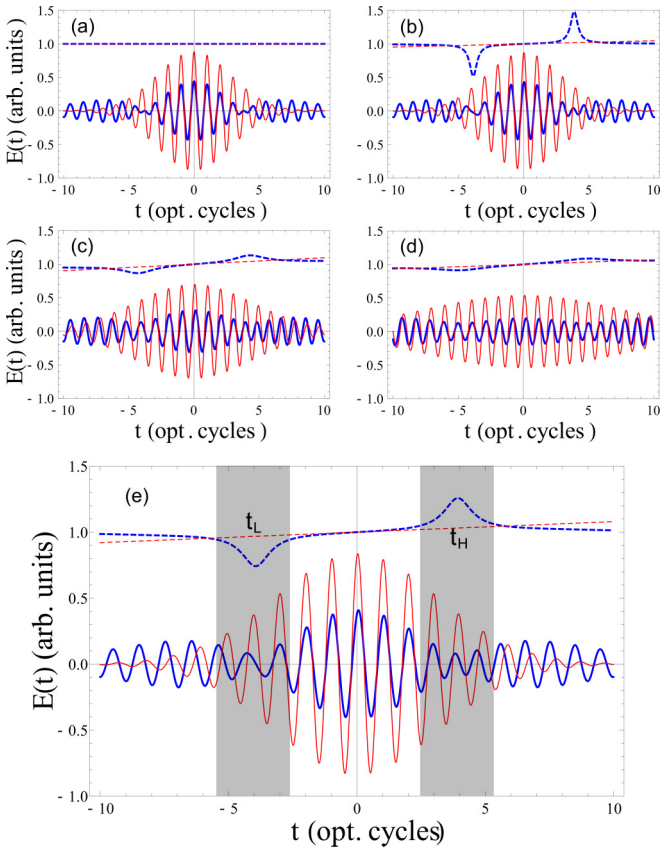

FIG. 1. Instantaneous frequencies $\omega^D_{\rm SB}(t)$ (blue dashed lines) and $\omega^D_G(t)$ (red dashed lines) normalized to the carrier frequency ω_0. Panels (a)–(e) correspond to different values of the parameter Ω which take in to account the propagation of the pulse through a DM: $\Omega = 0, 1, 5, 10$, and 2 opt. cycles^2, respectively. In addition, the corresponding fields $E^D_{\rm SB}(t)$ (blue solid lines) and $E^D_G(t)$ (red solid lines) are shown.

Our aim is to show the behavior of the instantaneous frequency of the SB pulse in the DM $[\omega^D_{\rm SB}(t)]$ and compare it with that of the Gaussian pulse $[\omega^D_G(t)]$. To this purpose, we calculate the expression in Eq. (4) for the set of values $\omega_0 = 2\pi$ and $\Delta\omega = 0.5$ (both in units of $\frac{\rm rad}{\rm opt.cycles}$), which corresponds to a Gaussian pulse $\tilde{E}_G(\omega)$ with a temporal FWHM, $\tau = \frac{2\sqrt{2ln2}}{\Delta\omega} \approx 5$ opt. cycles. These results are shown in Fig. 1, where we adopt the values $\alpha = 1$ and $\beta = 0.5$ for the synthesis parameters to obtain the SB pulse $\tilde{E}_{\rm SB}(\omega)$, while Ω was varied to take into account the effect of different media (GVD) and propagation distances (z): $\Omega = 0$ [Fig. 1(a)], $\Omega = 1$ [Fig. 1(b)], $\Omega = 5$ [Fig. 1(c)], and $\Omega = 10$ [Fig. 1(d)], all in units of opt. cycles^2. From these figures it can be seen that, while $\omega^D_G(t)$ has a linear behavior, $\omega^D_{\rm SB}(t)$ is almost constant except within two temporal windows that are localized, symmetrically, on either sides of $t = 0$. These local oscillations of the electric field $\tilde{E}^D_{\rm SB}(\omega)$, have a frequency value below and above the minimum and maximum values reached by $\omega^D_G(t)$, and we will refer to those frequencies as $\omega_{\rm low}$ and $\omega_{\rm high}$, respectively. Such oscillations tend to disappear when Ω increases, and $\omega^D_{\rm SB}(t)$ converges to $\omega^D_G(t)$.

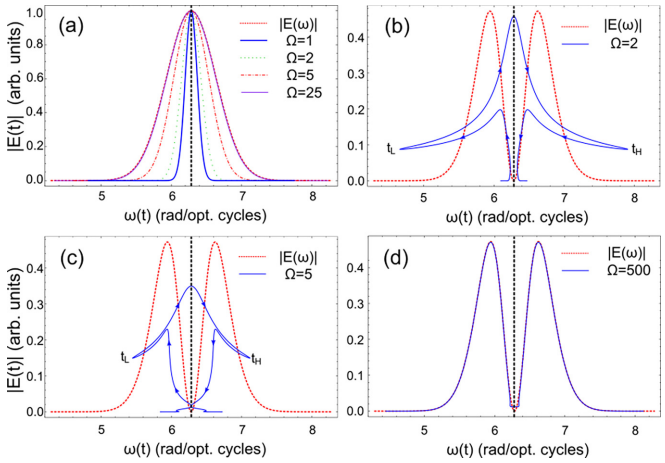

FIG. 2. Parametric curves $[\omega(t), |E(t)|]$ for a pulse propagating in a DM, and superimposed, the spectral amplitude $|\tilde{E}(\omega)|$ of the corresponding field. (a) Gaussian pulse $E_G^D(t)$. In panels (b)–(d) the field considered is that of the SB pulse $E_{\rm SB}^D(t)$. The arrows in (b,c) indicate the evolution of the parametric curve with time.

A more detailed visualization of the phenomenon is shown in Fig. 1(e). This figure is obtained for $\Omega = 2$ opt. cycles^2 and corresponds to high and low oscillations with frequency values $\omega_{\rm high} \sim 1.25\omega_0$ and $\omega_{\rm low} \sim 0.75\omega_0$, localized at $t = t_L = -3.95$ opt. cycles and $t = t_H = 3.95$ opt. cycles, respectively. The shadow regions indicate the temporal windows where this phenomenon occurs. In addition, it can be observed how the period of the field $E_{\rm SB}^D(t)$ (blue line) varies in relation to the period of $E_G^D(t)$ (red line). Finally, to estimate the weight of these oscillations, we calculate the amplitude ratios between the different fields: $|E_{\rm SB}^D(t_H)|/|E_{\rm SB}^D(0)| = 0.192$, $|E_{\rm SB}^D(t_H)|/|E_G^D(0)| = 0.094$, $|E_{\rm SB}^D(t_H)|/|E_G(0)| = 0.089$. As reference value, we can consider the weight in the Fourier spectrum of the Gaussian pulse at the frequency value $\omega = 1.25\omega_0$, which is given by $\tilde{E}_G(1.25\omega_0)/\tilde{E}_G(0) = e^{-(\frac{1.25\times 2\pi - 2\pi}{0.5})^2} = e^{-\pi^2} = 5.17\times 10^{-5}$. From all the proposed ways to quantify the weight of the frequency $\omega_{\rm high}$, this value is at least, three orders of magnitude greater than the value given by the Fourier spectrum. It should be noted that $|E_{\rm SB}^D(t_L)| = |E_{\rm SB}^D(t_H)|$, so the analysis is also valid for the frequency $\omega_{\rm low}$.

In Fig. 2, we show a set of parametric curves in the form $[\omega(t), |E(t)|]$, which allow a general quantification of the oscillations represented by $\omega(t)$. In addition, the corresponding spectral amplitude $|\tilde{E}(\omega)|$ is superimposed. Figure 2(a) corresponds to the parametric curves for the Gaussian pulse $E_G^D(t)$, propagating in a DM with $\Omega = 1, 2, 5$, and 25 opt. cycles^2. From this figure it can be observed how, as the pulse propagates through the medium, the parametric curves converges to the spectral amplitude $|\tilde{E}_G(\omega)|$. This result can be seen as equivalent to obtain the temporal Fourier transform, which does not provide information about localized events, by the GVD of the medium [24]. In Fig. 2(b), it is shown the parametric curve for the SB pulse propagating in a DM, $E_{\rm SB}^D(t)$, with $\Omega = 2$ opt. cycles^2 [the same example of Fig. 1(e)], where the arrows indicate the evolution of the curve with time. It is observed that the curve crosses the spectral amplitude $|\tilde{E}_{\rm SB}(\omega)|$ and the maximum distance between both occurs for $t = t_L$ and $t = t_H$, denoting the appearance of two localized oscillations, of significant weight that are clearly outside the Fourier spectrum of the pulse. From Fig. 2(c), we can see a similar behavior, now for the case with $\Omega = 5$ opt. cycles^2 [the same example of Fig. 1(c)], being the maximum distance to $|\tilde{E}_{\rm SB}(\omega)|$ shorter than in Fig. 2(b). Finally, in Fig. 2(d) we display the case with $\Omega = 500$ opt. cycles^2. Here, the shape of the parametric curve is quite similar to the shape of $|\tilde{E}_{\rm SB}(\omega)|$. As in the case of Fig. 2(a), when the pulse propagates enough through the medium, the temporal Fourier transform is obtained. In analogy with the spatial domain, where the far-field Fraunhofer diffraction is proportional to the spatial Fourier transform, we can conclude that the appearance of local oscillations at frequencies $\omega_{\rm high}$ and $\omega_{\rm low}$ occurs in the "temporal near field."

An estimate of the ranges in which a behavior like that of Fig. 1(e) is present in a realistic situation can be obtained, for example, by considering a fused silica glass whose GVD, at $\lambda_0 = 800$ nm ($T_0 \approx 2.7$ fs), is $\beta_2 = 36.163$ fs^2/mm. Since the dispersion length is defined as $L_D = \tau^2/|\beta_2|$, then $\Omega = \frac{1}{2}\beta_2 \times z = \frac{1}{2}\tau^2 \frac{z}{L_D}$. In our case, with $\Omega = 2$ opt. cycles^2 and $\tau = \frac{2\sqrt{2ln2}}{\Delta\omega} \approx 5$ opt. cycles, we find that $z/L_D = 2\Omega/\tau^2 = 4/25 = 0.16$, i.e., the pulse propagates in the medium $z = 0.16L_D \approx 0.8$ mm. In Appendix B, where the mathematical analysis of the frequency $\omega_{\rm SB}^D(t)$ is presented, it is shown that the appearance of these local oscillations occurs when $\Omega\Delta\omega^2 \approx 1$. In addition, other kinds of SB pulses are analyzed in Appendix C.

To study the effect of the DM on different SB pulses, in Fig. 3 we show the evolution of a pulse with the same synthesis parameter as the SB pulse analyzed up to this point, except for the value of the parameter α. As we showed in Ref. [22], the temporal FWHM of the central lobe of the pulse given by Eq. (1), decreases when the product $\alpha \times \beta$ increases and converges to zero when $\alpha \times \beta \to 1$. In our case, since $\beta = 0.5$, we vary α in the range $1 \leqslant \alpha < 1.9$. However, we consider that the SB pulse propagates in a medium with $\Omega = 2$ opt. cycles^2. From Figs. 3(a) ($\alpha = 1.1$), 3(b) ($\alpha = 1.3$), 3(c) ($\alpha = 1.6$), and 3(d) ($\alpha = 1.7$), it can be seen that the frequencies $\omega_{\rm high}$ and $\omega_{\rm low}$ (at t_H and t_L, respectively) increase, in absolute value with respect to ω_0, as α increases, up to a certain value for which the times t_H and t_L are reversed, and the opposite behavior is observed, i.e., the values of those frequencies begin to decrease when α increases. In Fig. 3(e), we show the case with $\alpha = 1.9$. A clear change in the behavior of $\omega_{\rm SB}^D(t)$ is observed with respect to the lower values of α. In a temporal region around $t = 0$, $\omega_{\rm SB}^D(t)$ can be approximated by a straight line with a negative slope, opposite to that of $\omega_G^D(t)$. The temporal position of the frequencies $\omega_{\rm high}$ and $\omega_{\rm low}$ are now inverted, i.e., $t_H < 0$ and $t_L > 0$. In other temporal regions the value of $\omega_{\rm SB}^D(t)$ remains constant. It is worth mentioning the similitude between the shape of $\omega_{\rm SB}^D(t)$ and the shape of the instantaneous frequency given by the phenomenon known as *self-phase modulation* [34]. The mathematical expression for the change in sign of the slope of $\omega_{\rm SB}^D(t)$ at $t = 0$ is analyzed in Appendix B.

To conclude, we highlight that the phenomena presented in this work extend to SB pulses synthesized from the

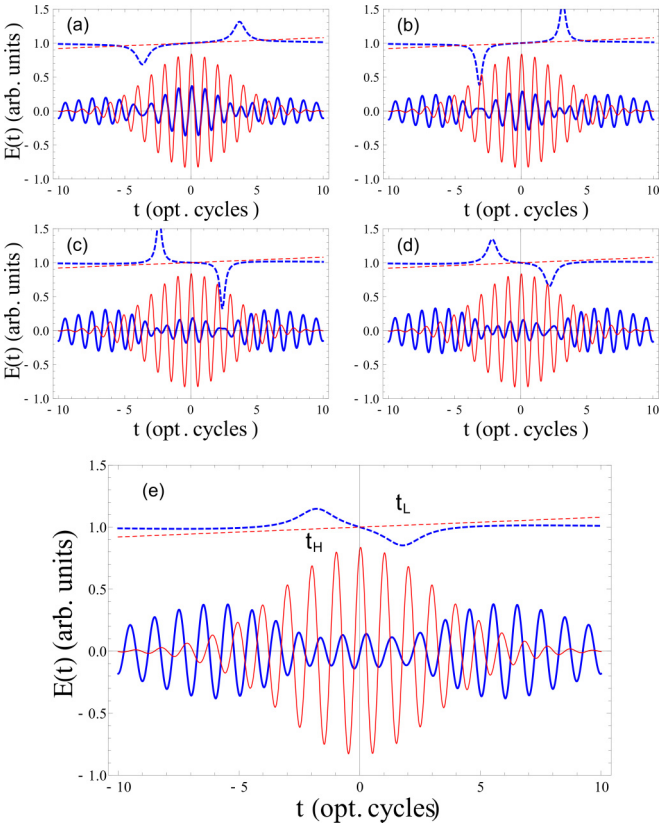

FIG. 3. Similar to Fig. 1, but for different values of the synthesis parameter α of the SB pulse [Eq. (1)]. Panels (a)–(e) correspond to $\alpha = 1.1$, 1.3, 1.6, 1.7, and 1.9, respectively. In all cases, the pulse propagates through a DM with $\Omega = 2$ opt. cycles^2.

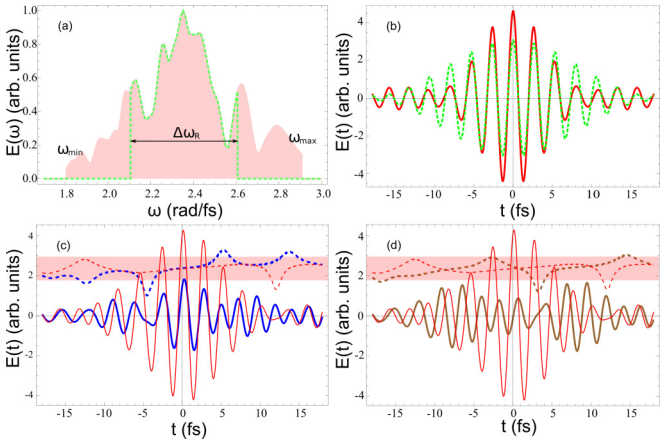

FIG. 4. (a) Fourier spectrum of the non-Gaussian pulse $\tilde{E}_{NG}(\omega)$ (pink region) and response of the rectangular spectral filter to obtain the pulse $\tilde{E}_R(\omega)$ (green dashed lines). (b) Pulses $E_{NG}(t)$ (red solid line) and $E_R(t)$ (green dashed line). (c) Instantaneous frequencies $\omega^D_{\rm SB}(t)$ (blue dashed line) and $\omega^D_{NG}(t)$ (red dashed line) for a synthesis parameter $\alpha = 0.85$, when the propagation length in the DM is $z = 300\,\mu$m. The pink region indicates the spectral content of $E_{NG}(t)$ [see Fig. 4(a)]. In addition, the propagating pulses $E^D_{\rm SB}(t)$ (blue solid line) and $E^D_{NG}(t)$ (red solid line) are shown. (d) Similar to (c) but for $\alpha = 1.37$. Here, $\omega^D_{\rm SB}(t)$ is displayed in brown dashed line and $E^D_{\rm SB}(t)$ in brown solid line.

coherent superposition of non-Gaussian ultrashort pulses, with a complex frequency spectrum. As a concrete example, in Fig. 4(a), we show the Fourier spectrum of a non-Gaussian pulse $\tilde{E}_{\rm NG}(\omega)$, which is centered at $\omega_C \approx 2.35$ rad/fs ($\lambda_C \approx 800$ nm) and limited between $\omega_{\rm min} \approx 1.8$ and $\omega_{\rm max} \approx 2.9$ rad/fs. The dashed green lines indicate the bandwidth $\Delta\omega_R$ of the spectral rectangular filter considered to obtain a second non-Gaussian pulse $\tilde{E}_R(\omega)$, which subsequently interferes with $\tilde{E}_{\rm NG}(\omega)$. Figure 4(b) corresponds to the temporal representation of the original pulse $E_{\rm NG}(t)$, and the pulse $E_R(t)$ broadened as a consequence of the spectral filtering. As previously shown, in the frequency domain the SB pulse is given by $\tilde{E}_{\rm SB}(\omega) = \tilde{E}_{\rm NG}(\omega) - \alpha\tilde{E}_R(\omega)$ [see Eq. (1)], and different synthesis result depending on the amplitude ratio α between both fields. Without loss of generality, we consider that the SB pulse propagates through a fused silica glass, so that $E^D_{\rm SB}(t) = \mathcal{F}[\tilde{E}_{\rm SB}(\omega)e^{-iK(\omega)\times z}]$, with $K(\omega) = \frac{\omega}{c}n_{\rm glass}(\omega)$, for which a fifth-order fit function in ω is considered, with $n_{\rm glass}(\omega)$ being the refractive index of the medium [23]. In Fig. 4(c), corresponding to $\alpha = 0.85$ and $z = 300\,\mu$m, the instantaneous frequency $\omega^D_{\rm SB}(t)$ reveals the presence of two local oscillations beyond the Fourier spectrum of the pulse $E_{\rm NG}(t)$, in the central region where the frequency $\omega^D_{\rm NG}(t)$ remains almost linear. Similar to what was seen in Fig. 1, $\omega^D_{\rm SB}(t)$ has a behavior consistent with a positive DM $\beta_2 > 0$. In the present example, unlike the previous one, a second pair of oscillations appear on either side of the central region, where $\omega^D_{\rm NG}(t)$ deviates from the linear behavior and also shows two side oscillations. However, these secondary oscillations have a negligible weight compared to the primary ones. Finally, in Fig. 4(d) which corresponds to $\alpha = 1.37$ and $z = 300\,\mu$m, the primary local oscillations exhibit the change in behavior previously observed in Fig. 3, that is, the slope of the instantaneous frequency change its sign as if the pulse had traveled through a medium with $\beta_2 < 0$.

III. CONCLUSION

We studied the superbandwidth phenomenon in laser pulses through the propagation characteristics of SB pulses in a DM. We showed the appearance of local oscillations of the electric field that are beyond the Fourier spectrum of the SB pulse. Here, the superoscillatory phenomenon and the complementary phenomenon of suboscillations [35] take place as part of a single phenomenon since they occur for the same SB pulse at the same propagation distance. For some ranges of values of the pulse synthesis parameters, these local oscillations behave as if they had traveled through a medium with a positive or negative GVD, beyond the dispersion properties of the material, behavior that is not expected to occur in linear media.

In addition to the direct application that these results could have for coherent control [36–38], pulse shaping [29,39,40], signal processing [41–43], and ultrafast spectroscopy [44–46], the concept of superbandwidth of a band-limited function can be extended to other wave phenomena. Moreover, the spatiotemporal coupling in ultrashort laser pulses could be the key to isolate, spatially, the local oscillations of the electric field given by its superbandwidth [47,48].

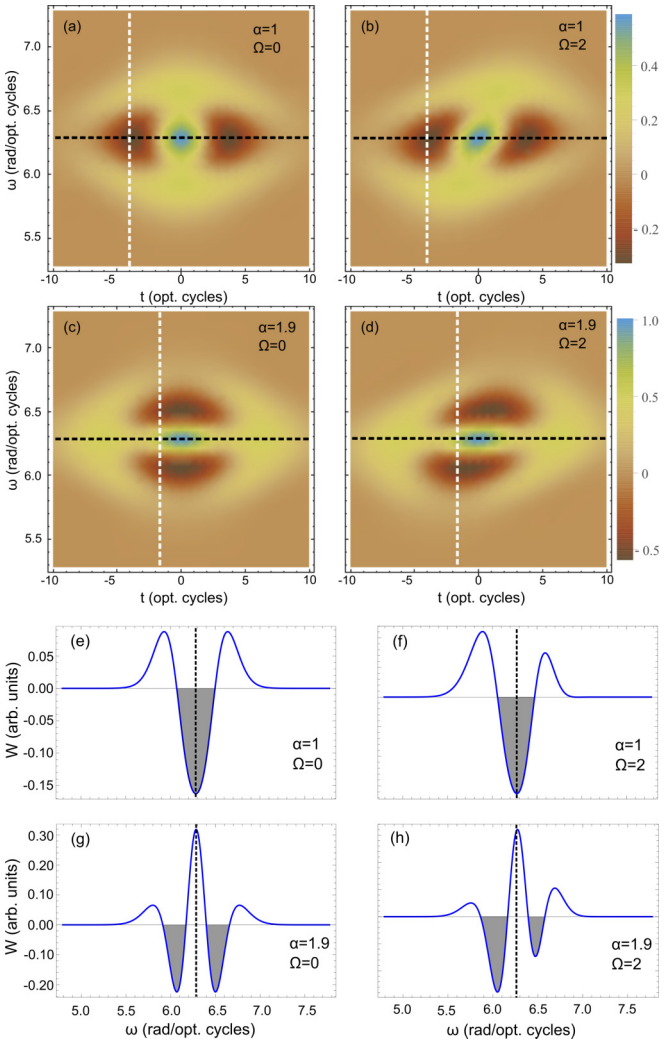

FIG. 5. Panels (a)–(d): Wigner function $W(t,\omega)$ of a propagating SB pulse. Panels (e,f) Cross section of the 2D map of $W(t,\omega)$ corresponding to the dashed white lines in panels (a) to (d), respectively.

ACKNOWLEDGMENTS

E.G.N. and L.R. acknowledge the Consejo Nacional de Investigaciones Científicas y Técnicas (CONICET). L.A.B.R. and P.A.C.C. acknowledge the CONICET and Comisión Nacional de Energía Atómica (CNEA). F.A.V. acknowledges to Comisión de Investigaciones Científicas de la Pcia. de Buenos Aires (CICPBA). This work was partially supported by the following projects: SIIP 2022-2024 06/C034 and 06/C033 of Universidad Nacional de Cuyo (UNCUYO), PICT-2020-SERIE-A-823 and PICT-2021-GRF-742 of Agencia Nacional de Promoción Científica y Tecnológica (ANPCyT), and red FFFLASH (Redes Federales de Alto Impacto) of MINCyT.

APPENDIX A: TIME-FREQUENCY ANALYSIS FROM THE WIGNER FUNCTION DISTRIBUTION

A different perspective of the underlying physics behind the phenomenon can be obtained from the analysis of the Wigner function distribution, which allows us to decompose the *superbandwidth* phenomenon in a time-frequency representation. To this end, in Fig. 5 we show the Wigner distribution $W(t,\omega)$ for a SB pulse, as obtained from Eq. (4) in the main text. Two SB pulses, with a different value of the parameter α, are considered. When the SB pulse travels through a medium with $\Omega = 0$, i.e., without dispersion, $W(t,\omega)$ exhibits a positive central lobe along two negative regions, horizontally or vertically aligned for the case with $\alpha = 1$ [Fig. 5(a)] or $\alpha = 1.9$ [Fig. 5(c)], respectively. In these cases, the negative values of $W(t,\omega)$ account for the destructive interference resulting from the coherent superposition of two Gaussian pulses [49], which results in the synthesis given by Eq. (2) of the main text. In addition, the Wigner distribution is symmetric with respect to both axes. However, when the pulse propagates in a dispersive medium [$\Omega = 2$ opt. cycles^2 for the examples that are shown in Figs. 5(b) and 5(d) corresponding to $\alpha = 1$ and $\alpha = 1.9$, respectively], such symmetry is broken. This breaking of the mirror symmetry of $W(t,\omega)$ originates from the time dependence of the instantaneous frequency $\omega(t)$. In Figs. 5(e) to 5(h), we show a cross section of the two-dimensional (2D) maps in Figs. 5(a) to 5(d), respectively, for a given value of $t = t^*$ (dashed white lines). From these figures, it becomes clear that since $\omega(t^*)$ is the average frequency weighted by $W(t^*,\omega)$, when $\Omega = 0$ the instantaneous frequency coincides with the carrier frequency [$\omega(t^*) = \omega_0$], independently of the negative values of $W(t^*,\omega)$ [Figs. 5(e) and 5(g)]. For $\Omega \neq 0$, the asymmetry of $W(t^*,\omega)$ causes the time dependence in $\omega(t)$, which can now reach higher and lower values than those given by the Fourier spectrum as a consequence of the negative values of $W(t^*,\omega)$ [50] (otherwise, a positive function distribution always has a first moment whose value is between the minimum and maximum values of the variable).

APPENDIX B: MATHEMATICAL ANALYSIS OF SB LASER PULSES PROPAGATING IN A DISPERSIVE MEDIUM.

The temporal representation of the real electric field of the initial Gaussian pulse can be described as $\mathrm{Re}[E_G(t)] = |E_G(t)|\cos(\omega_0 t)$. According to Eq. (2) of the main paper, which we replicate here to ease the derivation as Eq. (B1)

$$\tilde{E}_{\mathrm{SB}}(\omega) = e^{-(\frac{\omega-\omega_0}{\Delta\omega})^2} - \alpha e^{-(\frac{\omega-\omega_0}{\beta\Delta\omega})^2}, \tag{B1}$$

the complex fields of the initial pulse, which we rename here as $E_G(t) = E_1(t)$ to simplify the derivations, and modified pulse, $E_2(t)$ are, respectively,

$$E_1(t) = \frac{\Delta\omega}{2\sqrt{\pi}} e^{-\frac{(\Delta\omega t)^2}{4}} e^{i\omega_0 t}, \tag{B2}$$

$$E_2(t) = \beta\frac{\Delta\omega}{2\sqrt{\pi}} e^{-\frac{(\beta\Delta\omega t)^2}{4}} e^{i\omega_0 t}. \tag{B3}$$

Then, the SB pulse can be represented as

$$\begin{aligned} E_{\mathrm{SB}}(t) &= E_1(t) - \alpha E_2(t) \\ &= \frac{\Delta\omega}{2\sqrt{\pi}}(e^{-\frac{(\Delta\omega t)^2}{4}} - \alpha\beta e^{-\frac{(\beta\Delta\omega t)^2}{4}}) e^{i\omega_0 t}. \end{aligned} \tag{B4}$$

Considering a medium having second order dispersion (GVD) with transfer function $H_D(\omega) = e^{-i\Omega(\omega-\omega_0)^2}$, the real electric fields of both pulses traveling through such a

medium are

$$\begin{aligned}\mathrm{Re}[E_1^D(t)] &= |E_1^D(t)| \times \mathrm{Re}[e^{i\phi_1^D(t)}] \\ &= \frac{\Delta\omega}{2\sqrt{\pi}} \frac{e^{-\frac{(\Delta\omega t)^2}{4[1+(\Omega\Delta\omega^2)^2]}}}{[1+(\Omega\Delta\omega^2)^2]^{\frac{1}{4}}} \\ &\quad \times \cos\left(\omega_0 t + \frac{\Omega\Delta\omega^4}{4[1+(\Omega\Delta\omega^2)^2]} t^2 + \theta_1^D\right), \quad \text{(B5)} \\ \mathrm{Re}\big[E_2^D(t)\big] &= \big|E_2^D(t)\big| \times \mathrm{Re}[e^{i\phi_2^D(t)}] \\ &= \alpha\beta \frac{\Delta\omega}{2\sqrt{\pi}} \frac{e^{-\frac{(\beta\Delta\omega t)^2}{4[1+(\Omega\beta^2\Delta\omega^2)^2]}}}{[1+(\Omega\beta^2\Delta\omega^2)^2]^{\frac{1}{4}}} \\ &\quad \times \cos\left(\omega_0 t + \frac{\Omega\beta^4\Delta\omega^4}{4[1+(\Omega\beta^2\Delta\omega^2)^2]} t^2 + \theta_2^D\right), \end{aligned} \quad \text{(B6)}$$

where $\phi_1^D(t)$ and $\phi_2^D(t)$ are the corresponding chirps that the medium imprints on both pulses, $\theta_1^D = \frac{1}{2}\arctan(-\Omega\Delta\omega^2)$ and $\theta_2^D = \frac{1}{2}\arctan(-\Omega\beta^2\Delta\omega^2)$ are constant phase values, and $|E_1^D(t)|$ and $|E_2^D(t)|$ are the modulus of the dispersed fields with durations that increased by a factor of $\sqrt{1+(\Omega\Delta\omega^2)^2}$ and $\sqrt{1+(\Omega\beta^2\Delta\omega^2)^2}$, respectively.

The real electric field of the dispersed SB pulse can be written as

$$\mathrm{Re}\big[E_{\mathrm{SB}}^D(t)\big] = \big|E_1^D(t)\big|\cos\big(\phi_1^D(t)\big) - \alpha\big|E_2^D(t)\big|\cos\big(\phi_2^D(t)\big). \quad \text{(B7)}$$

By combining the two sinusoidal functions into a single one, the expression can be rearranged as

$$\begin{aligned}\mathrm{Re}\big[E_{\mathrm{SB}}^D(t)\big] &= \big|E_{\mathrm{SB}}^D(t)\big| \times \mathrm{Re}[e^{i\phi_{\mathrm{SB}}^D(t)}] \\ &= |E_{\mathrm{SB}}^D(t)| \cos\left(\frac{\phi_1^D(t)+\phi_2^D(t)}{2} + \Delta\phi(t)\right), \end{aligned} \quad \text{(B8)}$$

where $|E_{\mathrm{SB}}^D(t)|$ is the envelope of the real electric field of the dispersed SB pulse and $\Delta\phi(t)$ a phase term, both functions defined as

$$\begin{aligned}\big|E_{\mathrm{SB}}^D(t)\big|^2 &= \big|E_1^D(t)\big|^2 + |E_2^D(t)|^2 \\ &\quad - 2\alpha\big|E_1^D(t)\big|\big|E_2^D(t)\big| \cos\big(\phi_1^D(t) - \phi_2^D(t)\big), \\ \tan(\Delta\phi(t)) &= \frac{\big|E_1^D(t)\big| + \alpha\big|E_2^D(t)\big|}{\big|E_1^D(t)\big| - \alpha\big|E_2^D(t)\big|} \tan\left(\frac{\phi_1^D(t)-\phi_2^D(t)}{2}\right). \end{aligned} \quad \text{(B9)}$$

The phase of the dispersed SB pulse has the expression presented in Eq. (B15)

$$\begin{aligned}\phi_{\mathrm{SB}}^D(t) &= \frac{\phi_1^D(t)+\phi_2^D(t)}{2} + \arctan\left[\frac{\big|E_1^D(t)\big| + \alpha\big|E_2^D(t)\big|}{\big|E_1^D(t)\big| - \alpha\big|E_2^D(t)\big|} \tan\left(\frac{\phi_1^D(t)-\phi_2^D(t)}{2}\right)\right] \\ &= \omega_0 t + \left(\frac{1}{1+(\Omega\Delta\omega^2)^2} + \frac{\beta^4}{1+(\Omega\beta^2\Delta\omega^2)^2}\right)\frac{\Omega\Delta\omega^4 t^2}{8} + \frac{\theta_1^D+\theta_2^D}{2} \\ &\quad + \arctan\left\{\frac{\big|E_1^D(t)\big| + \alpha\big|E_2^D(t)\big|}{\big|E_1^D(t)\big| - \alpha\big|E_2^D(t)\big|} \tan\left[\left(\frac{1}{1+(\Omega\Delta\omega^2)^2} - \frac{\beta^4}{1+(\Omega\beta^2\Delta\omega^2)^2}\right)\frac{\Omega\Delta\omega^4 t^2}{8} + \frac{\theta_1^D-\theta_2^D}{2}\right]\right\}. \end{aligned} \quad \text{(B10)}$$

Differentiating the phase of the dispersed SB pulse we find its instantaneous frequency in Eq. (B11)

$$\omega_{\mathrm{SB}}^D(t) = \frac{d\phi_{\mathrm{SB}}^D(t)}{dt} = \omega_0 + \left(\frac{1}{1+(\Omega\Delta\omega^2)^2} + \frac{\beta^4}{1+(\Omega\beta^2\Delta\omega^2)^2}\right)\frac{\Omega\Delta\omega^4 t}{4} + \Delta\omega(t). \quad \text{(B11)}$$

It can be seen that the dispersed SB pulse has a main linear chirp as it would be expected for a dispersed single Gaussian pulse, but it also presents a deviation $\Delta\omega(t)$ that after many derivations can be expressed as

$$\Delta\omega(t) = \frac{\left(\big|E_1^D(t)\big|^2 - \big|E_2^D(t)\big|^2\right)\frac{1}{2}\left(\frac{d\phi_1^D(t)}{dt} - \frac{d\phi_2^D(t)}{dt}\right)}{\big|E_{\mathrm{SB}}^D(t)\big|^2} + \frac{\left(\big|E_1^D(t)\big|\frac{d|E_2^D(t)|}{dt} - \big|E_2^D(t)\big|\frac{d|E_1^D(t)|}{dt}\right)\sin\big(\phi_1^D(t)-\phi_2^D(t)\big)}{\big|E_{\mathrm{SB}}^D(t)\big|^2}. \quad \text{(B12)}$$

It can be analyzed the asymptotic behavior of $\omega_{\mathrm{SB}}^D(t)$ if the range of values when $|E_1^D(t)|$ becomes negligible, i.e., $|t|$ is greater than three times the standard deviation of the Gaussian pulse, is considered. In this case, $\frac{d|E_1^D(t)|}{dt}$ is also approximately zero, $|E_{\mathrm{SB}}^D(t)|^2 \approx \alpha^2|E_2^D(t)|^2$ and $\Delta\omega(t) \approx -\frac{1}{2}(\frac{d\phi_1^D(t)}{dt} - \frac{d\phi_2^D(t)}{dt})$, so the instantaneous frequency has the asymptotic expression of Eq. (B13)

$$\begin{aligned}\omega_{\mathrm{SB}}^D(t) &\approx \omega_0 + \frac{\Omega\beta^4\Delta\omega^4}{2[1+(\Omega\beta^2\Delta\omega^2)^2]}\, t, \\ |t| &> 3\frac{\sqrt{2}}{\Delta\omega}\sqrt{1+(\Omega\Delta\omega^2)^2}. \end{aligned} \quad \text{(B13)}$$

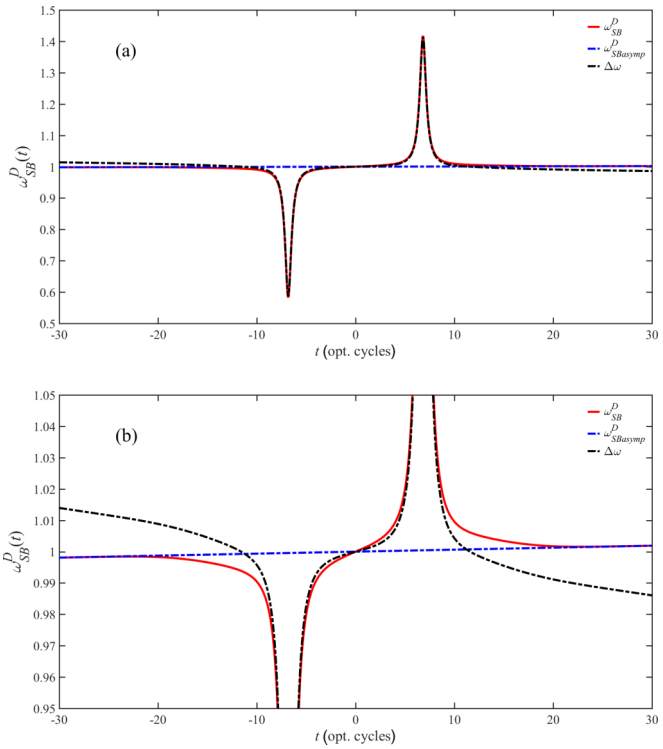

FIG. 6. Instantaneous frequency of the dispersed SB pulse normalized with respect to ω_0: (a) the complete amplitude range, (b) zoom in of the amplitude; $\omega^D_{\rm SB}(t)$ (solid red line), its asymptotic response (dashed blue line), $|\Delta\omega(t)|$ (dashed black line), with $\alpha = 1$, $\beta = 0.5$, and $\Omega = 2$.

The dispersed SB Gaussian pulse presents a linear chirp over the region of its tails governed by the instantaneous frequency of the dispersed modified Gaussian pulse $E^D_2(t)$. When $|t|$ decreases, the chirp of both dispersed pulse components, $E^D_1(t)$ and $E^D_2(t)$, start to interact and the behavior of $\omega^D_{\rm SB}(t)$ becomes more intricate as we approach to the region near t_L or t_H where $|E^D_{\rm SB}(t)|^2$ becomes greatly diminished and makes $\Delta\omega(t)$ to be highly increased with respect to ω_0. This effect can be appreciated in Fig. 6(a) where $\omega^D_{\rm SB}(t)$ and its asymptotic response are presented in solid red line and dashed blue line, respectively, together with $\Delta\omega(t)$ in the dashed black line for the same parameters of Fig. 1(e) of the main paper ($\alpha = 1$, $\beta = 0.5$, and $\Omega = 2$), all normalized with respect to ω_0.

In Fig. 6(b) we present a zoom in of the amplitude of the instantaneous frequency in Fig. 1(a). It can be appreciated in detail that if $|t|$ is further decreased, i.e., t values inside the central part of the dispersed SB pulse, the response of the instantaneous frequency is dominated by $\Delta\omega(t)$, meaning that, for low values of the α parameter, can be approximated by Eq. (B15)

$$\omega^D_{\rm SB}(t) \approx \omega_0 + \Delta\omega(t), \qquad |t| \lesssim |t_L|, |t_H|\,, \quad 0 < \alpha < 1. \tag{B14}$$

When higher values of the α parameter are considered, the complete expression of $\omega^D_{\rm SB}(t)$ should be analyzed.

Now it can be clearly understood the foundations of the local oscillations with frequency values that are below and above than those expected for a regular dispersed Gaussian pulse. Moreover, for particular synthesis parameters of the dispersed SB pulse, the instantaneous frequency reaches values beyond those expected by its Fourier transform. The expression of the instantaneous frequency deviation $\Delta\omega(t)$, which is inversely proportional to the squared real-valued envelope of the dispersed SB pulse $|E^D_{\rm SB}(t)|^2$, makes it possible to explain the appearance of these local oscillations, why they present an increased absolute value with respect to ω_0, and why their positions are in the range where the envelope has local minima.

In Figs. 3(a) through 3(d) of the main article, the evolution of a pulse with the same synthesis parameters, except for the value of α, was introduced. It was shown that the frequencies $\omega_{\rm high}$ and $\omega_{\rm low}$ (at t_H and t_L, respectively) increase, in absolute value with respect to ω_0, as α increases, up to a certain value for which the times t_H and t_L are reversed. This behavior can be easily understood due to a change of the sign in the numerator of the frequency deviation $\Delta\omega(t)$ because of its dependence on the parameter α, and remembering that the denominator, the squared real valued envelope $|E^D_{\rm SB}(t)|^2$, has a positive value. This particular value of α may be obtained, if the values of t_H or t_L are known, by calculating the roots of the quadratic polynomial present in the numerator of $\Delta\omega(t)$ when it is evaluated at t_H or t_L.

Finally, in Fig. 3(e) of the main paper it was shown that, for a value of $\alpha = 1.9$ ($\beta = 0.5$, $\Omega = 2$) in a temporal region around $t = 0$, the instantaneous frequency of the dispersed SB pulse can be approximated by a straight line with a negative slope, opposite to that present on a dispersed single Gaussian pulse. This surprising behavior where the local oscillations around $t = 0$ behave as if they had traveled through a medium with opposite sign GVD, beyond the dispersion properties of the material, start to happen, for a given dispersion value Ω, when α surpasses a critical value α_c. This particular value of α can be found by differentiating the instantaneous frequency and equating it to 0, while evaluating this expression for $t = 0$. By performing this procedure a quadratic function of α_c is obtained, which after proper mathematical manipulation, is shown as Eq. (B15)

$$\frac{\beta^6}{[1+(\Omega\beta^2\Delta\omega^2)^2]^{\frac{3}{2}}}\alpha_c^2 - \frac{1}{[1+(\Omega\Delta\omega^2)^2]^{\frac{1}{4}}}\frac{1}{[1+(\Omega\beta^2\Delta\omega^2)^2]^{\frac{1}{4}}}\left[\left(\frac{1}{1+(\Omega\Delta\omega^2)^2}+\frac{\beta^4}{1+(\Omega\beta^2\Delta\omega^2)^2}\right)\cos(\Delta\theta^D)\right.$$
$$\left. - \frac{1}{\Omega\Delta\omega^2}\left(\frac{1}{1+(\Omega\Delta\omega^2)^2}-\frac{\beta^2}{1+(\Omega\beta^2\Delta\omega^2)^2}\right)\sin(\Delta\theta^D)\right]\beta\alpha_c + \frac{1}{[1+(\Omega\Delta\omega^2)^2]^{\frac{3}{2}}} = 0, \tag{B15}$$

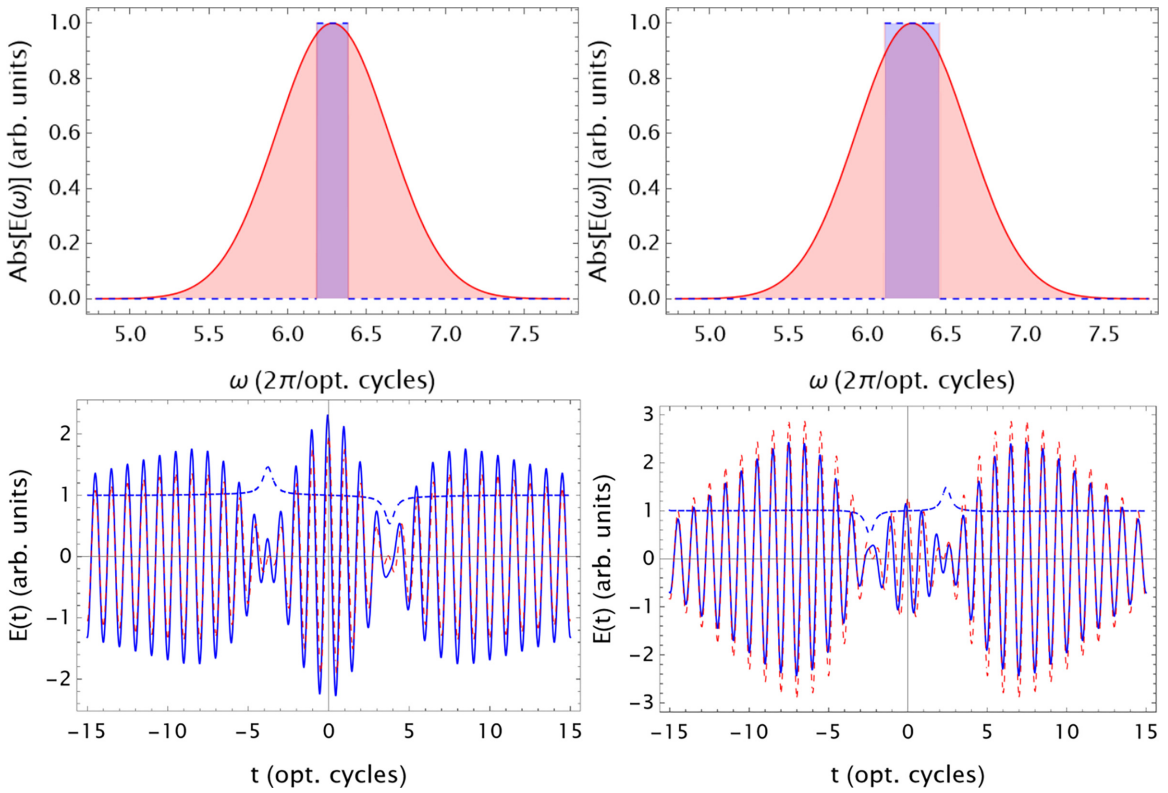

FIG. 7. (Top panels) Absolute value of the spectral field $|\tilde{E}_{\mathrm{SB1}}(\omega)|$ in red region and the spectral phase $\mathrm{Arg}[\tilde{E}_{\mathrm{SB1}}(\omega)]/\pi$ blue region. The left panel correspond to $r = 0.4$ and the right panel correspond to $r = 0.7$. (Bottom panels) Real part of the temporal fields $E_{\mathrm{SB1}}(t)$ in dashed red line, $E^{D}_{\mathrm{SB1}}(t)$ in blue line, and the instantaneous frequency $\omega^{D}_{1}(t) = \frac{d\mathrm{Arg}[E^{D}_{\mathrm{SB1}}(t)]}{dt}/2\pi$ in dashed blue line. The left panel correspond to $r = 0.4$ and the right panel correspond to $r = 0.7$. The value of the dispersion for both panels is $\Omega = 2$ opt. cycles^2.

where $\Delta\theta^{D} = \theta^{D}_{1} - \theta^{D}_{2} = \frac{1}{2}\arctan(-\Omega\Delta\omega^2) - \frac{1}{2}\arctan(-\Omega\beta^2\Delta\omega^2) = \frac{1}{2}\arctan(\frac{-\Omega\Delta\omega^2(1-\beta^2)}{1+\Omega^2\beta^2\Delta\omega^4})$. The roots of Eq. (B15) will present two values of α_c, and typically the lower root will be below 2 for $\beta = 0.5$ which represents a practical value for the dispersed modified pulse ($\alpha\beta < 1$).

It should be noted that the phenomenon is clearly evident when the pulse is propagated through a dispersive medium with length $z \lesssim L_D$, which means that the initial Gaussian pulse is spread temporally twice or less. This spreading of the Gaussian pulse is given by an increase in its duration of $\sqrt{1 + (\Omega\Delta\omega^2)^2}$. By considering $\Omega\Delta\omega^2 = 1$, the temporal spreading becomes $\sqrt{2}$, determining a clear compromise relation between Ω and $\Delta\omega$ for which the phenomenon occurs. If we consider a modified pulse with $\beta = 0.5$, a value of $\alpha_c = 1.593$. This means that for values of $\alpha > 1.593$ there is a change of the sign of the instantaneous frequency slope at $t = 0$, as if the central part of the pulse had traveled through a medium with a second order dispersion opposite to that of the actual medium.

APPENDIX C: OTHER KINDS OF SB LASER PULSES

In this section we will show two other kinds of SB pulses propagating in a dispersive medium, characterized by the operator $H_D(\omega) = e^{-i\Omega(\omega-\omega_0)^2}$.

The first SB pulse to be analyzed, described by the field $\tilde{E}_{\mathrm{SB1}}(\omega)$, is a Gaussian pulse to which a π-phase mask is printed [51]. Mathematically, such a mask is represented by the operator $H_\pi(\omega) = e^{i\pi\times\mathrm{rect}(\frac{\omega-\omega_0}{r\Delta\omega})}$, where the rectangular function $\mathrm{rect}(x/x_0)$ is defined as

$$\mathrm{rect}(x/x_0) = \begin{cases} 1 & \text{if } |x| \leqslant x_0/2, \\ 0 & \text{if } |x| > x_0/2. \end{cases} \tag{C1}$$

Thus, we can write the field $\tilde{E}_{\mathrm{SB1}}(\omega)$ as follows:

$$\tilde{E}_{\mathrm{SB1}}(\omega) = e^{-\left(\frac{\omega-\omega_0}{\Delta\omega}\right)^2} e^{i\pi\times\mathrm{rect}\left(\frac{\omega-\omega_0}{r\Delta\omega}\right)}, \tag{C2}$$

where the parameters ω_0 and $\Delta\omega$ represent, as in the Eq. (1) of the main paper, the carrier frequency and the bandwidth of the pulse. The parameter r indicates the region where a phase shift equal to π occurs. In the time space, by varying the parameter r, a pulse with sub-Fourier characteristics in its temporal width is obtained [51].

We considered here the same values of the pulse parameters ω_0 and $\Delta\omega$ of the initial Gaussian pulse $\tilde{E}_G(\omega)$ in the main paper, i.e., $\omega_0 = 2\pi$ and $\Delta\omega = 0.5$, which correspond to a FWHM of $\tau = \frac{2\sqrt{2\ln 2}}{\Delta\omega} \approx 5$ opt. cycles. In Fig. 7 the top panels show the field $\tilde{E}_{\mathrm{SB1}}(\omega)$ with $r = 0.4$ and $r = 0.7$, indicating the spectral field amplitude $|\tilde{E}_{\mathrm{SB1}}(\omega)|$ in red, while colored in blue the region where the phase change equal to π occurs. The bottom panels show the real part of the temporal fields $E_{\mathrm{SB1}}(t)$ (dashed red line), $E^{D}_{\mathrm{SB1}}(t)$ (blue line), and the instantaneous frequency $\omega^{D}_{1}(t) = \frac{d}{dt}(\mathrm{Arg}[E^{D}_{\mathrm{SB1}}(t)])$ normalized to the carrier frequency ω_0 (dashed blue line). The left panel (right panel)

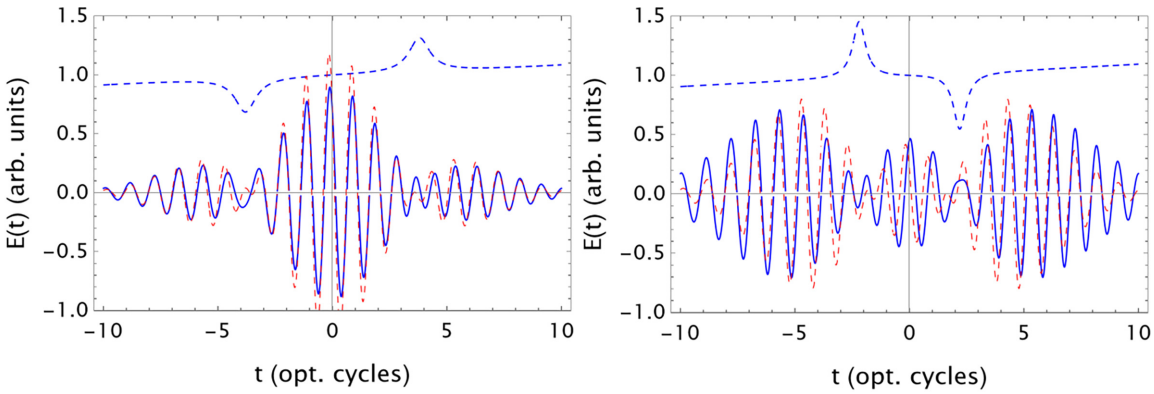

FIG. 8. Real part of the temporal field $E_{\mathrm{SB1}}(t)$ [$E^{D}_{\mathrm{SB1}}(t)$] in dashed red line (blue solid line). In dashed blue line, the instantaneous frequency $\omega^{D}_{1}(t) = \frac{d\mathrm{Arg}[E^{D}_{\mathrm{SB1}}(t)]}{dt}$ normalized to the carrier frequency ($\omega_0 = 2\pi$), is shown. Left panel corresponds to the case with with $\alpha = 0.9$, $\beta_D = 2$ opt. cycles^2, and $\Omega = 1$ opt. cycle^2. In the right panel, the value of the parameter α was increased to 1.02.

corresponds to pulses with $r = 0.4$ ($r = 0.7$) in a dispersive medium with $\Omega = 2$ opt. cycles^2. From these figures, the same behavior of the instantaneous frequency shown in the Figs. 1 and 3 of the main paper can be seen, i.e., the appearance of local oscillations beyond the Fourier spectrum of the pulse (left panel), and also the phenomenon in which the behavior changes as if the dispersion of the medium changed its sign.

The second SB pulse, $\tilde{E}_{\mathrm{SB2}}(\omega)$, is that studied in Ref. [21] for which a destructive interference between two Gaussian pulses with different temporal widths is reached by printing a quadratic phase (chirp) into one of those pulses. The similitude between the field $\tilde{E}_{\mathrm{SB2}}(\omega)$ and the field $\tilde{E}_{\mathrm{SB}}(\omega)$ analyzed in the main paper [Eq. (1) in the main paper], are analyzed in Ref. [19]. This SB pulse can be written as

$$\tilde{E}_{\mathrm{SB2}}(\omega) = e^{-(\frac{\omega-\omega_0}{\Delta\omega})^2} + \alpha e^{i\phi_D(\alpha,\beta_D)} e^{-(\frac{\omega-\omega_0}{\Delta\omega})^2} e^{-i\beta_D(\omega-\omega_0)^2}, \tag{C3}$$

where β_D is the chirp parameter. For this SB pulse, the condition of destructive interference is achieved for a phase difference $\phi_D(\alpha, \beta_D)$ (see Refs. [19,20]). In the left panel of Fig. 8 is shown the real part of the temporal field $E_{\mathrm{SB2}}(t)$, with $\alpha = 0.9$ and $\beta_D = 2$ opt. cycles^2 (dashed red line), the dispersed SB pulse, $E^{D}_{\mathrm{SB2}}(t)$, with $\Omega = 1$ opt. cycle^2 (blue line), and the instantaneous frequency, $\omega^{D}_{2}(t) = \frac{d}{dt}(\mathrm{Arg}[E^{D}_{\mathrm{SB2}}(t)])$ (dashed blue line). In the right panel we replicate these plots but for a different value of the parameter α ($\alpha = 1.02$ in this case). Again, in these figures can be appreciated the same behavior of the instantaneous frequency shown in the Figs. 1 and 3 of the main paper.

It is worth mentioning that both fields, $E_{\mathrm{SB1}}(t)$ and $E_{\mathrm{SB2}}(t)$, have their own characteristics when they propagate in a dispersive medium, which depend on their respective synthesis parameters, and are different from those of the field $E_{\mathrm{SB}}(t)$ studied in the main paper.

[1] M. Berry, N. Zheludev, Y. Aharonov, F. Colombo, I. Sabadini, D. C. Struppa, J. Tollaksen, E. T. Rogers, F. Qin, M. Hong *et al.*, Roadmap on superoscillations, J. Opt. **21**, 053002 (2019).

[2] M. Berry and S. Popescu, Evolution of quantum superoscillations and optical superresolution without evanescent waves, J. Phys. A: Math. Gen. **39**, 6965 (2006).

[3] Y. Aharonov, F. Colombo, I. Sabadini, D. Struppa, and J. Tollaksen, *The Mathematics of Superoscillations* (American Mathematical Society, Providence, RI, 2017), Vol. 247.

[4] N. I. Zheludev and G. Yuan, Optical superoscillation technologies beyond the diffraction limit, Nat. Rev. Phys. **4**, 16 (2022).

[5] K. Cheng, Z. Li, J. Wu, Z.-D. Hu, and J. Wang, Super-resolution imaging based on radially polarized beam induced superoscillation using an all-dielectric metasurface, Opt. Express **30**, 2780 (2022).

[6] Z. Wu, F. Dong, S. Zhang, S. Yan, G. Liang, Z. Zhang, Z. Wen, G. Chen, L. Dai, and W. Chu, Broadband dielectric metalens for polarization manipulating and superoscillation focusing of visible light, Acs Photon. **7**, 180 (2020).

[7] K. Zhang, H. Jiang, F. Dong, H. Hu, Z. Song, L. Xu, Z. Shang, G. Liang, Z. Zhang, Z. Wen *et al.*, Generating ultralong-superoscillation nondiffracting beams with full control of the intensity profile, Phys. Rev. Appl. **19**, 014041 (2023).

[8] P. J. S. Ferreira and A. Kempf, Superoscillations: Faster than the nyquist rate, IEEE Trans. Signal Process. **54**, 3732 (2006).

[9] Y. Luo, Z. Zhan, X. Wang, and J. Wang, Creation and preservation of superoscillation in a dielectric optical waveguide, Opt. Lett. **48**, 1176 (2023).

[10] Y. Eliezer, L. Hareli, L. Lobachinsky, S. Froim, and A. Bahabad, Breaking the temporal resolution limit by superoscillating optical beats, Phys. Rev. Lett. **119**, 043903 (2017).

[11] G. McCaul, P. Peng, M. O. Martinez, D. R. Lindberg, D. Talbayev, and D. I. Bondar, Superoscillations deliver super-spectroscopy, Phys. Rev. Lett. **131**, 153803 (2023).

[12] S. Brehm, A. V. Akimov, R. P. Campion, and A. J. Kent, Temporal superoscillations of subterahertz coherent acoustic phonons, Phys. Rev. Res. **2**, 023009 (2020).

[13] Y.-X. Shen, Y.-G. Peng, F. Cai, K. Huang, D.-G. Zhao, C.-W. Qiu, H. Zheng, and X.-F. Zhu, Ultrasonic super-oscillation wave-packets with an acoustic meta-lens, Nat. Commun. **10**, 3411 (2019).

[14] G. Chen, Z.-Q. Wen, and C.-W. Qiu, Superoscillation: from physics to optical applications, Light Sci. Appl. **8**, 56 (2019).

[15] M. Lin, J. Li, D. Zhang, B. Ratni, J. Yi, P. Qi, K. Zhang, A. de Lustrac, and S. N. Burokur, Reconfigurable near-field focusing reflector based on superoscillation mechanism, *IEEE Antennas*

and Wireless Propagation Letters, (IEEE, New York, 2023), Vol. 22.

[16] M. R. Dennis, A. C. Hamilton, and J. Courtial, Superoscillation in speckle patterns, Opt. Lett. **33**, 2976 (2008).

[17] G. H. Yuan, S. Vezzoli, C. Altuzarra, E. T. Rogers, C. Couteau, C. Soci, and N. I. Zheludev, Quantum super-oscillation of a single photon, Light Sci. Appl. **5**, e16127 (2016).

[18] Y. Eliezer and A. Bahabad, Super-transmission: The delivery of superoscillations through the absorbing resonance of a dielectric medium, Opt. Express **22**, 31212 (2014).

[19] E. G. Neyra and P. Vaveliuk, Tailoring a sub-diffraction optical focus via a straightforward interferometric approach, J. Opt. **23**, 075604 (2021).

[20] E. G. Neyra, G. A. Torchia, P. Vaveliuk, and F. Videla, Simple interferometric setup enabling sub-fourier-scale ultra-short laser pulses, J. Opt. **24**, 045504 (2022).

[21] E. G. Neyra, D. A. Biasetti, P. Vaveliuk, G. A. Torchia, M. F. Ciappina, F. Videla, and L. Rebón, Effective super-bandwidth in laser pulses, Opt. Lett. **46**, 4761 (2021).

[22] E. G. Neyra, D. A. Biasetti, F. Videla, L. Rebón, and M. F. Ciappina, Principal frequency, superbandwidth, and low-order harmonics generated by superoscillatory pulses, Phys. Rev. Res. **4**, 033254 (2022).

[23] J.-C. Diels and W. Rudolph, *Ultrashort Laser Pulse Phenomena* (Elsevier, Amsterdam, 2006).

[24] T. Jannson, Real-time fourier transformation in dispersive optical fibers, Opt. Lett. **8**, 232 (1983).

[25] K. Goda and B. Jalali, Dispersive Fourier transformation for fast continuous single-shot measurements, Nat. Photon. **7**, 102 (2013).

[26] R. Fork, O. Martinez, and J. Gordon, Negative dispersion using pairs of prisms, Opt. Lett. **9**, 150 (1984).

[27] D. Strickland and G. Mourou, Compression of amplified chirped optical pulses, Opt. Commun. **55**, 447 (1985).

[28] F. Kärtner, N. Matuschek, T. Schibli, U. Keller, H. Haus, C. Heine, R. Morf, V. Scheuer, M. Tilsch, and T. Tschudi, Design and fabrication of double-chirped mirrors, Opt. Lett. **22**, 831 (1997).

[29] A. M. Weiner, Ultrafast optical pulse shaping: A tutorial review, Opt. Commun. **284**, 3669 (2011).

[30] I. Walmsley, L. Waxer, and C. Dorrer, The role of dispersion in ultrafast optics, Rev. Sci. Instrum. **72**, 1 (2001).

[31] T. Brabec and H. Kapteyn, *Strong Field Laser Physics* (Springer, New York, 2008), Vol. 1.

[32] J. Azaña, Time-Frequency (Wigner) analysis of linear and nonlinear pulse propagation in optical fibers, EURASIP J. Adv. Signal Process. **2005**, 314203 (2005).

[33] J. O.-C. neda, J. Lancis, C. M. Gómez-Sarabia, V. Torres-Company, and P. Andrés, Ambiguity function analysis of pulse train propagation: Applications to temporal Lau filtering, J. Opt. Soc. Am. A **24**, 2268 (2007).

[34] E. Neyra, F. Videla, J. Pérez-Hernández, M. F. Ciappina, L. Roso, and G. A. Torchia, Extending the high-order harmonic generation cutoff by means of self-phase-modulated chirped pulses, Laser Phys. Lett. **13**, 115303 (2016).

[35] Y. Eliezer and A. Bahabad, Super defocusing of light by optical sub-oscillations, Optica **4**, 440 (2017).

[36] T. Rybka, M. Ludwig, M. F. Schmalz, V. Knittel, D. Brida, and A. Leitenstorfer, Sub-cycle optical phase control of nanotunnelling in the single-electron regime, Nat. Photon. **10**, 667 (2016).

[37] Y.-M. He, H. Wang, C. Wang, M.-C. Chen, X. Ding, J. Qin, Z.-C. Duan, S. Chen, J.-P. Li, R.-Z. Liu *et al.*, Coherently driving a single quantum two-level system with dichromatic laser pulses, Nat. Phys. **15**, 941 (2019).

[38] Z. X. Koong, E. Scerri, M. Rambach, M. Cygorek, M. Brotons-Gisbert, R. Picard, Y. Ma, S. I. Park, J. D. Song, E. M. Gauger, and B. D. Gerardot, Coherent dynamics in quantum emitters under dichromatic excitation, Phys. Rev. Lett. **126**, 047403 (2021).

[39] C. Manzoni, O. D. Mücke, G. Cirmi, S. Fang, J. Moses, S.-W. Huang, K.-H. Hong, G. Cerullo, and F. X. Kärtner, Coherent pulse synthesis: Towards sub-cycle optical waveforms, Laser Photon. Rev. **9**, 129 (2015).

[40] E. Ridente, M. Mamaikin, N. Altwaijry, D. Zimin, M. F. Kling, V. Pervak, M. Weidman, F. Krausz, and N. Karpowicz, Electro-optic characterization of synthesized infrared-visible light fields, Nat. Commun. **13**, 1111 (2022).

[41] F. Krausz and M. I. Stockman, Attosecond metrology: from electron capture to future signal processing, Nat. Photon. **8**, 205 (2014).

[42] D. G. Lee and P. J. S. Ferreira, Superoscillations of prescribed amplitude and derivative, IEEE Trans. Signal Process. **62**, 3371 (2014).

[43] D. G. Lee and P. J. Ferreira, Superoscillations with optimal numerical stability, IEEE Signal Process. Lett. **21**, 1443 (2014).

[44] M. Maiuri, M. Garavelli, and G. Cerullo, Ultrafast spectroscopy: State of the art and open challenges, J. Am. Chem. Soc. **142**, 3 (2020).

[45] A. L. Cavalieri, N. Müller, T. Uphues, V. S. Yakovlev, A. Baltuška, B. Horvath, B. Schmidt, L. Blümel, R. Holzwarth, S. Hendel *et al.*, Attosecond spectroscopy in condensed matter, Nature (London) **449**, 1029 (2007).

[46] J. Shah, *Ultrafast Spectroscopy of Semiconductors and Semiconductor Nanostructures* (Springer Science & Business Media, New York, 2013).

[47] H. Vincenti and F. Quéré, Attosecond lighthouses: How to use spatiotemporally coupled light fields to generate isolated attosecond pulses, Phys. Rev. Lett. **108**, 113904 (2012).

[48] S. Akturk, X. Gu, P. Bowlan, and R. Trebino, Spatio-temporal couplings in ultrashort laser pulses, J. Opt. **12**, 093001 (2010).

[49] M. A. Alonso, Wigner functions in optics: describing beams as ray bundles and pulses as particle ensembles, Adv. Opt. Photon. **3**, 272 (2011).

[50] M. Berry and N. Moiseyev, Superoscillations and supershifts in phase space: Wigner and husimi function interpretations, J. Phys. A: Math. Theor. **47**, 315203 (2014).

[51] Y. Eliezer, B. K. Singh, L. Hareli, A. Arie *et al.*, Experimental realization of structured super-oscillatory pulses, Opt. Express **26**, 4933 (2018).